Synergistic antibacterial activity and inhibition of TiO$_2$ nanotube arrays and loaded antibiotics against gram-positive and gram-negative bacteria

Emmanuel Einyat Opolot[1], Haochen Wang[2],
Jeffrey R. Capadona[1,3], Horst A. von Recum[1] and
Hoda Amani Hamedani[3,4]*

[1]Department of Biomedical Engineering, Case Western Reserve University, Cleveland, OH, United States,
[2]Department of Electrical, Computer, and Systems Engineering, Case Western Reserve University,
Cleveland, OH, United States, [3]Advanced Platform Technology Center, Louis Stokes Cleveland Veterans
Affairs Medical Center, Cleveland, OH, United States, [4]Department of Materials Science and Engineering,
Case Western Reserve University, Cleveland, OH, United States

Introduction: Implantable medical devices continue to be vulnerable to bacterial infections. The unrelenting formation of antibiotic resistant bacterial strains not only exacerbates these infections but also renders the current treatment strategies impotent. The need is greater than ever for innovative and effective approaches to counteract drug-resistant bacteria. This study examines the innate antibacterial properties of TiO$_2$ nanotube arrays (TNAs) and their ability to locally deliver antibiotics to inactivate gram-positive and gram-negative bacteria, *in vitro*.

Methods: Using a two-step electrochemical anodization process, TNAs with a diameter of ~100 nm and a length of ~5 µm were grown on titanium substrates.

Results and Discussion: After 24 h of incubation, as-fabricated TNAs showed 100% clearance of *Escherichia coli*, and 97% clearance of *Staphylococcus aureus* growth. The antibiotic-loaded TNAs demonstrated sustained slow-release of cefotaxime and imipenem measured over 14 days. *In vitro* bacterial studies revealed the capability of cefotaxime- and imipenem-loaded TNAs in completely inhibiting the growth with 100% clearance of *Klebsiella pneumoniae* after 24 and 48 h of incubation. Bacterial inhibition assay revealed a significantly enlarged inhibition zone difference of 18 mm around the imipenem-loaded TNAs against *K. pneumoniae* compared to the as-fabricated TNAs which was maintained for 7 days with ~10 µgmL^{-1} of antibiotic released from the TNAs which was found to be lower than the dose required to completely eradicate multidrug resistant bacteria when used in conjunction with the antibacterial TNAs. The results of our study highlight the potential of TNAs as a versatile platform for addressing treatment strategies related to bacterial infections and antibiotic resistance in implantable medical devices.

KEYWORDS

antibacterial activity, TiO$_2$ nanotube arrays, local drug delivery, antibiotics, drug-resistant

1 Introduction

Bacterial infections continue to pose major global health concerns, specifically in implantable medical devices (Doron and Gorbach, 2008; VanEpps and Younger, 2016). These infections contribute to a substantial burden of morbidity and mortality worldwide (von Eiff et al., 2005a). Bacterial infections typically manifest as diseases such as pneumonia, as well as urinary tract infections and sepsis, which are often associated with surgically implanted medical devices such as catheters, vascular grafts, orthopedic and dental implants (Khatoon et al., 2018; von Eiff et al., 2005b). One of the potential causes of biomedical implant failure is an infection contracted during surgery or after healing. *Escherichia coli (E. coli)*, a Gram-negative bacterium, *S. aureus (Staphylococcus aureus)*, a Gram-positive bacteria, and *K. pneumoniae (Klebsiella pneumoniae)*, a Gram-negative bacteria, are among the commonly identified bacteria that cause such infections (Bao et al., 2012). Several treatment strategies have been used to combat implant-related bacterial infections. Systemic antibiotics are commonly used in post-surgery treatments after a medical device is implanted (Von Eiff et al., 2005a; Jepsen and Jepsen, 2016). However, systemic delivery of antibiotics via the bloodstream cannot achieve appropriate local concentrations in some areas of the body, such as at vascular-compromised locations (ter Boo et al., 2015). In addition, systemic administration of antibiotics at high concentrations may result in systemic toxicity problems if done for a long period of time. Despite the extensive reliance on antibiotics to treat bacterial illnesses, their effectiveness has also been undermined by the advent of drug-resistant bacterial strains and alteration of the composition and population of existing, stable strains of bacteria (Pray, 2008; Bassetti and Righi, 2020). Specifically, antibiotic resistance is a new challenge found to be higher in device-associated infections and has intensified the threat to public health (Martinez and Baquero, 2000; Medina and Pieper, 2016; Costa et al., 2020). *Klebsiella pneumoniae*, in particular, has gained attention as increasingly relevant clinical bacterial species for its high pathogenicity and ability to develop extreme resistance to multiple antibiotics (Costa et al., 2020).

Over the past 25 years, there has been notable stagnation in the development of novel antibiotics to manage the increasing prevalence of drug-resistant bacterial infections. A major cause of antibiotic resistance is the ability of organisms to form biofilms on medical devices (Fair and Tor, 2014; Khatoon et al., 2018). Biofilms form when bacteria are able to grow unchecked, and bacteria present in such biofilms have decreased vulnerability to antibiotics. Due to this pervasiveness of drug-resistant bacteria, implantable devices have become even more vulnerable to bacterial colonization. This is aggravated by the increasing rate of non-compliance with antibiotic therapy. Further, the inefficiencies of the currently predominant oral route of delivery of antibiotics, upsurge patient susceptibility to bacterial infections (Popat, Leoni, et al., 2007; Z.-L. Wu et al., 2020). Therefore, there is a huge drive for local sustained drug-delivery systems, independent of the patient and enhance targeting of bacteria at the sites of infection, at minimum inhibitory concentrations, without causing systemic side effects (Sekhon and Sekhon, 2021).

Aside from the treatment-based pharmacologic approaches, there has been remarkable progress in preventive strategies with the development of antibacterial materials and coatings that are designed to mitigate infections associated with implantable devices (L. Chen et al., 2020; Cyphert and von Recum, 2017; Darouiche, 2007). When applied to various implants, such coatings create surfaces with inherent antibacterial properties that act as a protective barrier against bacterial adhesion, colonization, and biofilm formation. Topographical features at micro- and nanoscale and surface roughness elicit antibacterial properties via a variety of mechanisms, which operate by either inhibiting bacterial adhesion or killing adhered bacterial cells (Baptista et al., 2018; Makabenta et al., 2021). However, the effect of other conditions, such as differences in the bacterial species tested and mediums used in experiments, need to be accounted for in the precise evaluation of the effects of topographical parameters (Zheng et al., 2021). Nanotechnology has also been critical in the development of antimicrobial coatings. It has enabled the development of nanomaterials with unique physico-chemical properties and tunable size, shapes and morphologies, as well as surface chemistry that influences their therapeutic activity. The use of nanomaterials may evade existing bacterial resistance mechanisms and result in less resistance selection than conventional antibiotics (Makabenta et al., 2021; Hetta et al., 2023). Various types of nanomaterials, including metal and metal oxide nanoparticles, carbon nanotubes, and graphene have all been investigated as bacterial resistant substrates (Dizaj et al., 2014; JankauskaitL et al., 2016). However, their effectiveness has primarily been tested against a limited spectrum of drug-resistant bacteria (Bowden et al., 2023).

In the wake of increasing bacterial adaptation and emergence of drug-resistant bacterial strains, a multi-pronged approach is desirable to leverage the combined effect of the antibacterial materials and the antibiotic drugs. Titanium dioxide (TiO_2) has emerged as a widely investigated biocompatible material for biomedical applications. TiO_2 is well-known for its non-toxicity and corrosion resistance, as well as its various antimicrobial properties, making it an ideal material for applications combating bacterial infections (Benčina et al., 2020; Jafari et al., 2020; Kumaravel et al., 2021). The exceptional properties of TiO_2 are further enhanced when they are formed as vertically aligned nanotube arrays (named as TiO_2 nanotube arrays or TNAs) (Roy et al., 2011; Jafari et al., 2020). An additional, unique feature of the nanotube arrays is their ability to store and locally deliver sustained release of a variety of therapeutic molecules (Gulati et al., 2015; Wang et al., 2016). This key characteristic is achieved when the nanotubes have a pore size relative to the size of drug molecule (Popat et al., 2007b). Due to the specific surface structure of TNAs and their ability to release drugs (such as antibiotics), they offer a competitive advantage over conventional therapies for treating infections caused by medical devices implanted in the body (Kunrath et al., 2019).

Several studies have concentrated on enhancing the antibacterial capabilities of TiO_2 nanotubes, primarily through surface modification by doping with metals like silver (Ag) and incorporating nanoparticles (Zhao et al., 2011; Mei et al., 2014). Additionally, there has been significant exploration into employing these nanotubes for active drug delivery in biomedical applications, integrating antibiotics such as gentamicin and vancomycin for targeted delivery (Popat et al., 2007a; Popat et al., 2007b; Draghi

et al., 2020). However, the effectiveness of these modifications has shown variability, with antibacterial activity limited to conventional laboratory bacteria and not including multidrug resistant bacteria. In this paper, we explore this innovative experimental strategy with TNAs for combating both conventional *S. aureus* and *E. coli* and multidrug resistant *K. pneumoniae,* a bacterium known for its significant role in post-surgical infections. We highlight the technology's potential in 1) addressing high-risk bacterial contaminants effectively, 2) the seamless integration of a drug delivery mechanism to synergistically enhance the antibacterial efficacy against clinically relevant bacterial strains. These findings not only underscore the versatility and significant potential for application of this technology as a protective antimicrobial coating for implantable medical devices, but also emphasize the adaptability and considerable promise of the TNAs to revolutionize antimicrobial approaches for prevention and treatment of implant-associated bacterial infections and drug resistance.

2 Materials and methods

2.1 Fabrication and characterization of TNAs

A two-step electrochemical anodization was used to form TNAs on Ti sheets. High-purity polished titanium foils (25 μm thick, 99.98%, Sigma-Aldrich) were sonicated in deionized (D.I.) water, ethanol and isopropyl alcohol (IPA), separately, and then dried in air. The anodization was performed in a two-electrode set-up containing an electrolyte mixture of 0.5 wt% of ammonium fluoride (NH$_4$F), 3 vol% of D.I. water and 96 vol% of ethylene glycol (EG) with Ti as the anode and the platinum foil (99.99%, Sigma-Aldrich) as the cathode. The first anodization was performed at 40 V for 30 min. Then, the nanotubes were removed by sonicating the sample in IPA for 5 min or until the nanotube layer is completely detached from the Ti substrate prior to the second anodization which was performed at 40 V for 100 min. The surface morphology of the films was observed using Apreo two scanning electron microscope (SEM). The surface morphology and chemical composition of the nanotube samples were analyzed using Apreo 2 (Thermo Fisher Scientific) scanning electron microscope (SEM) equipped with energy-dispersive X-ray spectroscopy (EDS). The surface roughness was measured using Veeco Dimension 3,100 atomic force microscopy (AFM) in tapping mode in air. The nanotube samples were analyzed using a 0.01–0.025 Ω.cm Antimony (n) doped Si cantilever with a force constant of 42 N/m, and at a resonance frequency of 320 kHz. The root-mean-square (RMS) roughness for surface topography was calculated on the basis of an average of 1×1 μm^2 height scans collected from three to five different positions on a representative image of the sample.

2.2 Antibiotics loading and release rate measurements

Antibiotic loading into samples was performed by pipetting a 22 mM solution of cefotaxime (Sodium Salt) and imipenem (APExBIO) dissolved in DI water, onto the surface of two coupons of TNA samples (nanotube length ~5 μm and areas of ~24 mm^2 and 28 mm^2, respectively). The cefotaxime and imipenem solutions were

pipetted onto the surface of each nanotubes sample via multiple pipetting steps to partially fill the nanotubes with the drug molecules. During these steps, the solution did not spill over the surface. Following each loading step, the solution penetrated the nanotubes, and the solvent was allowed to evaporate for 1 h ensuring that the nanotube array surface was completely dry prior to each pipetting and the release studies. Drug-loaded samples were immersed in Eppendorf tubes containing 100 μL of PBS (1X phosphate buffered saline) and were tightly closed to avoid evaporation. The tubes were placed in a water bath kept at 37°C. The concentrations of the released cefotaxime and imipenem were obtained via absorption measurements on three 2.5 μL drops from each sample tube using a Nanodrop One Microvolume UV-Vis Spectrophotometer at 260 and 297 nm, respectively. After each measurement, the entire PBS solution was replaced with 100 μL of fresh PBS to simulate the *in vivo* sink conditions. Daily measurements were taken for 14 days. Standard (calibration) curves with known concentrations of cefotaxime and imipenem were used to determine the unknown concentrations of the drug in the released medium.

2.3 Bacterial assays

2.3.1 Preparation of agar plates for bacteria

For the preparation of solid BBL agar plates (*E. coli,* and *S. aureus*) and nutrient agar plates (*K. pneumoniae*), trypticase powder broth (7.5 g) and granulated agar powder (15 g), and nutrient agar powder broth (23 g) (Fisher Scientific) was added to 180 mL and 1.0 L of distilled water, respectively. Both agar media were stirred (while heating for nutrient agar) till dissolved and autoclaved at 121°C for 20 min. The BBL and nutrient agar media were then respectively dispensed into Petri-dishes to air-dry under sterile conditions. BBL and nutrient agar plates were para-filmed and stored at 4°C until required for use.

2.3.2 Preparation of liquid broth for bacteria

For the preparation of the liquid broth, 7.5 g BBL trypticase broth powder (Fisher Scientific) was dissolved in 500 mL distilled water, stirred till dissolved, and then the content was sterilized by autoclaving for 20 min at 121°C. The liquid broth was allowed to cool and then stored at 4°C until required for use.

2.3.3 Bacterial cultures

The cultures were prepared by inoculating bacteria into 5 mL of BBL broth in a test tube. a two-step disinfected wire loop was used to transfer bacteria stock into the cold liquid broth under sterile conditions. The bacteria cultures grown include *E. coli* (*E. coli*) and *S. aureus* (*S. aureus*), donated by Dr. Ed Greenfield–Case Western Reserve University), and *K. pneumoniae* (*K. pneumoniae*), American Type Culture Collection (ATCC). A 150 μL of bacteria culture at initial concentrations of ~4.2 × 10^{10} CFU. mL^{-1} for *E. coli*, ~1.6 × 10^{11} CFU. mL^{-1} for *S. aureus*, and ~1.54 × 10^9 CFU. mL^{-1} for *Klebsiella pneumonia* was added to each snap top micro-vials (0.370 mL snap top polypropylene microvials, L&A Plastic Molding) with and without TNAs (positive controls). The initial concentration of *K. pneumoniae* for antibiotic-loaded TNAs was 1.23 × 10^{10} CFU. mL^{-1}. The micro-vials and their contents were incubated overnight in a 37°C shaker incubator at a constant agitation at 200 rpm. For serial dilution, 100 μL of

incubated culture was transferred into Eppendorf tubes with 900 μL of sterilized distilled water (DiH₂O). The bacteria samples were vortexed and then a constant volume (70 μL) was added onto the agar plates and spread over the plate using a sterile spreader. The agar plates were then incubated overnight at 37°C. The bacteria growth was observed by visual inspection of the plates and counting of colony-forming units (CFU).

2.3.4 Zone of inhibition assay

The inhibition zone against *K. pneumoniae* growth was determined using a modified zone of inhibition assay for the as-fabricated and imipenem-loaded TNA samples (n = 3). First, two-step anodized Ti discs with TNAs on both sides and a radius ~6 mm were prepared, three of which were loaded by pipetting 40 μL of imipenem solution (5 mg imipenem dissolved in 1 mL D.I. water) on one side. A *K. pneumoniae* culture was prepared overnight. Using a sterile procedure, 50 μL of *K. pneumoniae* culture was evenly spread over nutrient agar plates. The as-fabricated and imipenem-loaded TNA samples were placed (with the imipenem-loaded side facing down) in the middle of the plate on the fresh lawn of *K. pneumoniae* using sterile tweezers. The plates were incubated for 24 h at 37°C along with other optimal conditions for bacterial growth. After the incubation, the radius of the inhibition zone circle around each sample was measured at four different points using a dial-caliper and pictures of samples were captured. The TNA samples were left on the same agar plates for 7 days and the daily zone of inhibition measurements were performed with the images of the samples captured after every measurement. At the end of the assay, all samples were removed from the plates to observe the bacteria growth under the sample. Inhibition zone and its variation over time was identified by plotting the average radii of the *n* = 3 samples for each of the as-fabricated and imipenem-loaded TNA groups *versus* time.

2.3.5 Live/dead assay

The antibacterial activity of both as-fabricated and imipenem-loaded TNAs against *K. pneumoniae* was visually demonstrated using a modified live/dead assay. Briefly, a hazy culture of *K. pneumoniae* was grown in BBL broth overnight. The culture was serially diluted 3-fold in Milli Q water and sub-cultured for 8 h in BBL Broth, incubated at 37°C with both as-fabricated, and Imipenem-loaded TNAs (control not incubated with TNAs) in a shaker incubator. The live/dead bacteria cells were retrieved by centrifugation at 10,000 x g for 7 min at room temperature. The live/dead cells were resuspended in PBS. To stain the cells, 3 μL of a combined solution of 50 μL SYSTO 9 and 50 μL propidium iodide (PI) molecular probes (LIVE/DEAD BacLight bacterial viability kit, Thermo Fisher Scientific) were added to each milliliter of the live/dead cells and incubated for 10 min. The stained live/dead cells were visualized in a 96 well plate (100 μL aliquoted in each well plate) using a Zeiss Axio Z1 microscope (Colibri seven light source), with ×20 magnification, and the exposure time of 25 and 200 milliseconds for SYSTO nine and PI, respectively.

2.4 Statistical analysis

Where applicable, the ANOVA single factor analysis of variance was used to calculate the statistical differences and $p < 0.05$ was considered statistically significant. Data are expressed as mean ± standard deviation (SD) for *n* = 3 samples per group.
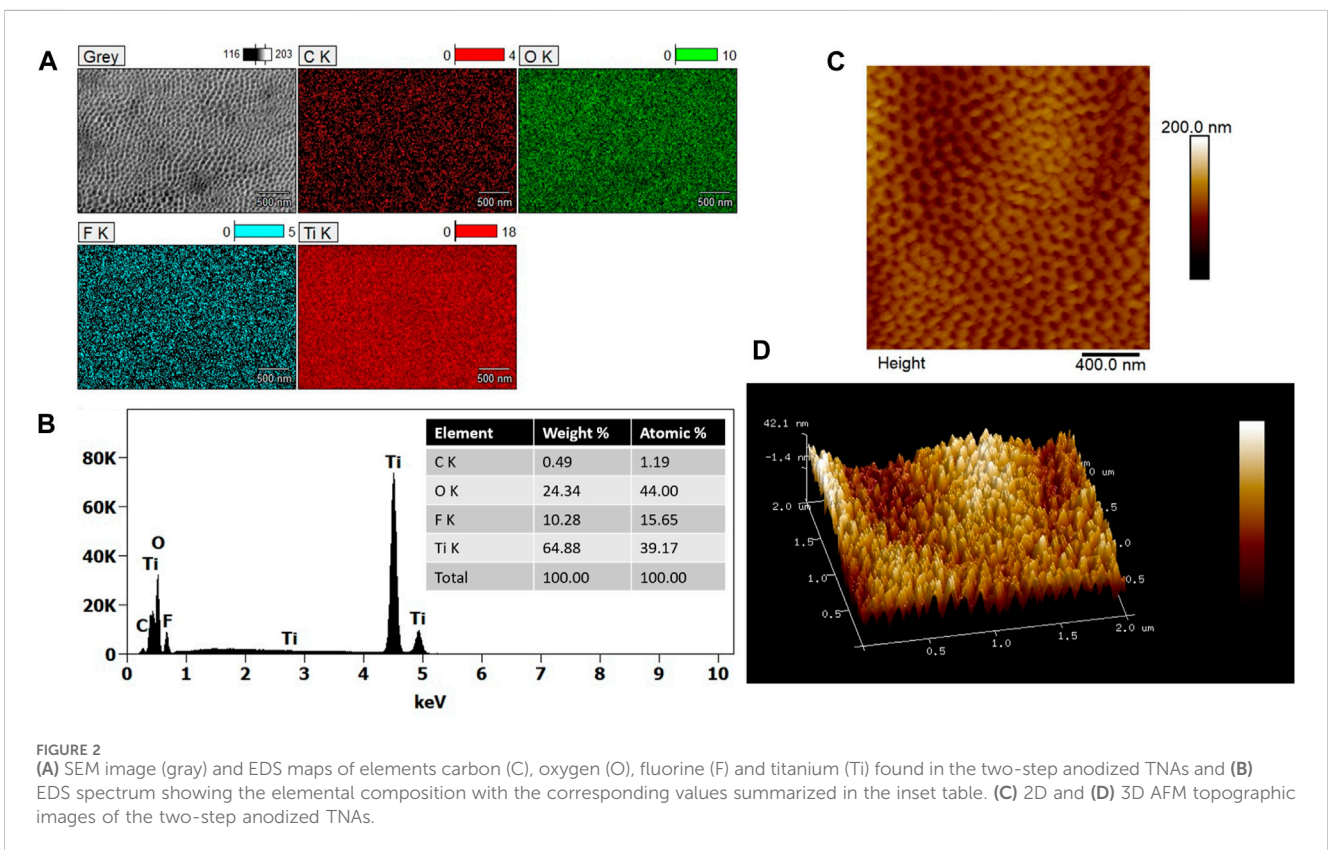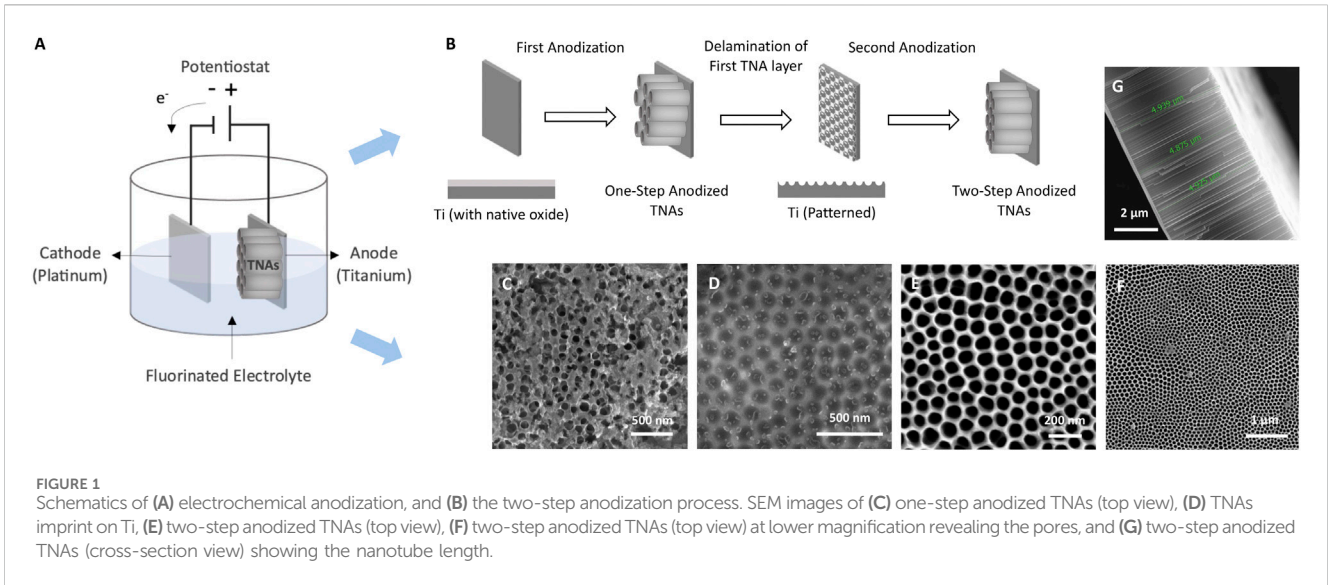
3 Results

3.1 Fabrication and characterization of TNAs

Figures 1A, B show the schematics of the electrochemical anodization setup and the two-step anodization process in a non-aqueous electrolyte. As can be seen in SEM image of the one-step anodized TNAs (Figure 1C), the first anodization of Ti foil at 40 V, for 30 min produced nanotubes with a non-uniform surface morphology. After the first anodization, the nanotube layer was delaminated and removed via sonication and the nanotubes imprint in the form of hexagonally packed spherical pits were remained on Ti substrate (Figure 1D). These pits were used as the starting point for the growth of nanotubes during the second step of anodization which resulted in the formation of debris-free highly ordered TNAs with smoother surface as compared to one-step anodized nanotubes (Figure 1C) with pore diameter of ~100 nm and tube length of ~5 μm after anodizing the patterned Ti foil at 40 V, for 100 min (Figures 1E–G).

According to EDS analysis (Figures 2A, B), the chemical composition of two-step anodized TNAs revealed a uniform distribution of titanium (Ti), oxygen (O), fluorine (F) and carbon (C) as shown in the EDS maps (Figure 2A). The presence of fluorine (~15 At.%) in TNAs is due to the use of fluoride containing electrolyte in the anodization process. Figures 2C, D shows the 2D and 3D AFM topographic images of the two-step anodized TNAs. The average surface root-mean-square roughness (R_q) of this sample was 12.6 ± 1 nm, which was found to be slightly lower than that of the one-step anodized TNAs in our study (14.5 ± 4).

3.2 *In Vitro* cumulative release of antibiotics from TNAs

Cefotaxime and imipenem are both considered as small molecules with low molecular weights (455.47 g mol⁻¹ mol and 299.347 g mol⁻¹, respectively). In this study, each antibiotic was separately loaded into TNA samples to evaluate their release from TNA samples. Based on the calculated volume of the available empty space in the nanotubes and the density of the drug molecules, the drug loading capacity of the 5 μm long TNAs was determined to be 2.25 μg mm⁻² for cefotaxime (density: 0.5 g cm³) and 7.2 μg mm⁻² for imipenem (density: 1.6 g cm³). Figure 3 shows *in vitro* cumulative release rate profiles of cefotaxime (Figure 3A) and imipenem (Figure 3B) from TNA samples at 37°C having nanotubes of ~100 nm-diameter pore size. For both cefotaxime- and imipenem-loaded TNAs, the release measurements were conducted for up to 14 days. After placing both samples in 1 X PBS, the first data point was obtained at $t_1 = 30$ min. Initially, non-zero release at $t_1 = 30$ min indicates fast diffusion of drug molecules due to high concentration gradients between TNA interface and PBS solution. Furthermore, this may result from the dissolution of the drug on TNA surfaces. According to these data, TNA samples released ~53 ng mm⁻² cefotaxime and ~48 ng mm⁻² imipenem within the first 30 min of release study and reach to ~58 ng mm⁻² cefotaxime and ~64 ng mm⁻² imipenem total release on day 14. The release values were reported in the unit of mass eluted in nanograms normalized to the "sample area" or "ng. mm⁻²"; as a result, it is possible to estimate the area of TNAs needed to coat implanted microdevices to deliver antibiotics with a desired dosage.

FIGURE 1
Schematics of **(A)** electrochemical anodization, and **(B)** the two-step anodization process. SEM images of **(C)** one-step anodized TNAs (top view), **(D)** TNAs imprint on Ti, **(E)** two-step anodized TNAs (top view), **(F)** two-step anodized TNAs (top view) at lower magnification revealing the pores, and **(G)** two-step anodized TNAs (cross-section view) showing the nanotube length.

FIGURE 2
(A) SEM image (gray) and EDS maps of elements carbon (C), oxygen (O), fluorine (F) and titanium (Ti) found in the two-step anodized TNAs and **(B)** EDS spectrum showing the elemental composition with the corresponding values summarized in the inset table. **(C)** 2D and **(D)** 3D AFM topographic images of the two-step anodized TNAs.

3.3 Bactericidal activity of as-fabricated TNAs

The antibacterial activity of as-fabricated TNAs were evaluated against a selected group of the most common Gram-positive and Gram-negative multidrug-resistant bacteria that cause infection-related implant failures (Bao et al., 2012). Figure 4 shows the antibacterial activity of the as-fabricated TNAs against *E. coli*, *S. aureus, and K. pneumoniae*. In these tests, ~30 mm^2 TNA samples were separately incubated with 150 μL of freshly inoculated bacteria of each type for 24 h (Figure 4A). At the 24-h timepoint, the bacteria were plated on BBL agar plates (for *E. coli*, and *S. aureus*) and nutrient agar plates (for *K. pneumoniae*). As shown in the results, as-fabricated TNAs completely eradicated the *E. coli* (100% clearance)
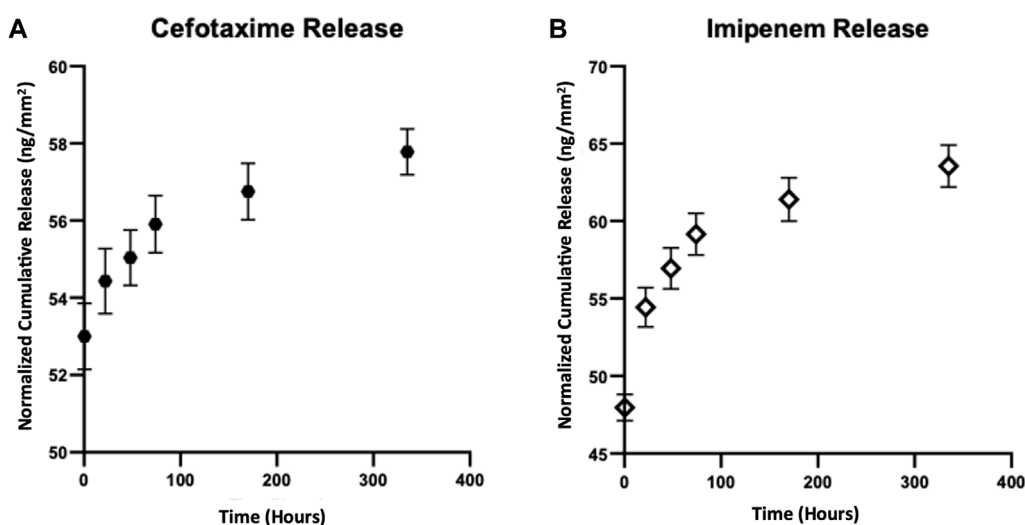
FIGURE 3
In vitro cumulative release rate profiles of **(A)** cefotaxime and **(B)** imipenem from TNA samples at 37°C. The release data shows the normalized cumulative release averaged over three measurements and obtained from TNA samples with ~5 μm-long nanotubes and ~100 nm-diameter pores for ~14 days. Data are expressed as mean ± standard deviation (*n* = 3).

(Figures 4B, E) and significantly abated *S. aureus* (97% clearance) (Figures 4C, F), but they showed less bactericidal activity against *K. pneumoniae* (80% clearance) in comparison to the other two types of bacteria (Figures 4D, G).

3.4 The synergistic antibacterial activity of antibiotic-loaded TNAs against *Klebsiella pneumoniae*

Here, we quantitatively tested the efficacy of cefotaxime and imipenem as antibiotics loaded into TNAs against *K. pneumoniae*. Figure 5A shows the antibacterial assay performed on TNA samples with a diameter of ~100 nm, a nanotube length of ~5 μm, and areas of ~24 and 28 mm², which were loaded with cefotaxime and imipenem, respectively, and were separately incubated with 150 μL of freshly inoculated bacteria (*K. pneumoniae*) for 24 and 48 h. The results showed that the localized release of cefotaxime and imipenem from TNAs can completely eradicate the growth of *K. pneumoniae* (100% clearance) after 24 h and 48 h of incubation (Figures 5B–E). From the *in vitro* release data shown in Figure 3, the measured eluted amount of cefotaxime from the TNA samples with the above areas were found to be 1.29 and 1.31 μg at 24 and 48 h timepoints, respectively. The total eluted amount of imipenem at these time points were found to be 1.54 and 1.61 μg. Considering the release volume of 150 μL, the concentrations of the antibiotics in the vials after 24 and 48 h of incubation were found to be 8.6 μg mL^{-1} and 8.73 μg mL^{-1} for cefotaxime and 10.27 and 10.73 μg mL^{-1} for imipenem.

3.5 Live/dead assay

The live/dead assay was conducted and reflected the effect of the TNAs on *K. pneumoniae* bacteria. Samples were compared to living bacteria cells (control) visualized by a green fluorescence from the SYSTO 9 as in (Figure 6Ai). Bacterial death in the presence of TNAs was revealed visually by a red fluorescence from the PI molecular probe. Figure 6Aii showed bacteria killed after 8 h of incubation with as-fabricated TNAs. Figure 6Aiii showed bacteria killed from the synergistic antibacterial activity of Imipenem-loaded TNAs after the same incubation time (8 h) as indicated by red/yellow (dead bacteria cells) vs green (live bacteria cells) in control.

3.6 Inhibition zone of as-fabricated and antibiotic-loaded TNAs against *Klebsiella pneumoniae*

The inhibition zone for *K. pneumoniae* growth was determined for the as-fabricated and imipenem-loaded TNA samples (*n* = 3) and its variation was recorded over time (for 7 days) as shown in Figures 6B–D. The inhibition zone size was identified as the radius of the circular area around TNA discs in which bacteria are unable to grow (Figures 6Bi–iii, Ci–iii). At the end of the assay (day 7), TNA samples were removed from the agar plates. No bacterial growth was found underneath the samples at the contact area with agar plate in both as-fabricated and imipenem-loaded TNA groups (Figures 6Biv, Civ). More importantly, the inhibition zone sizes were found to be significantly enlarged (~6 times larger radii) in imipenem-loaded compared to as-fabricated TNA samples (Figure 6D). These results confirmed that the TNAs not only prevented the growth of *K. pneumoniae* underneath them, but they also largely inhibited the bacteria growth in a well-defined area surrounding the samples via slow-release of the antibiotic. The zone of inhibition size for imipenem-loaded and as-fabricated TNA samples against *K. pneumoniae* was 21.23 ± 0.23 mm and 3.50 ± 0.32 mm, which was reduced to 19.05 ± 0.55 mm and 3.27 ± 0.06 mm, respectively, over 7 days of incubation.
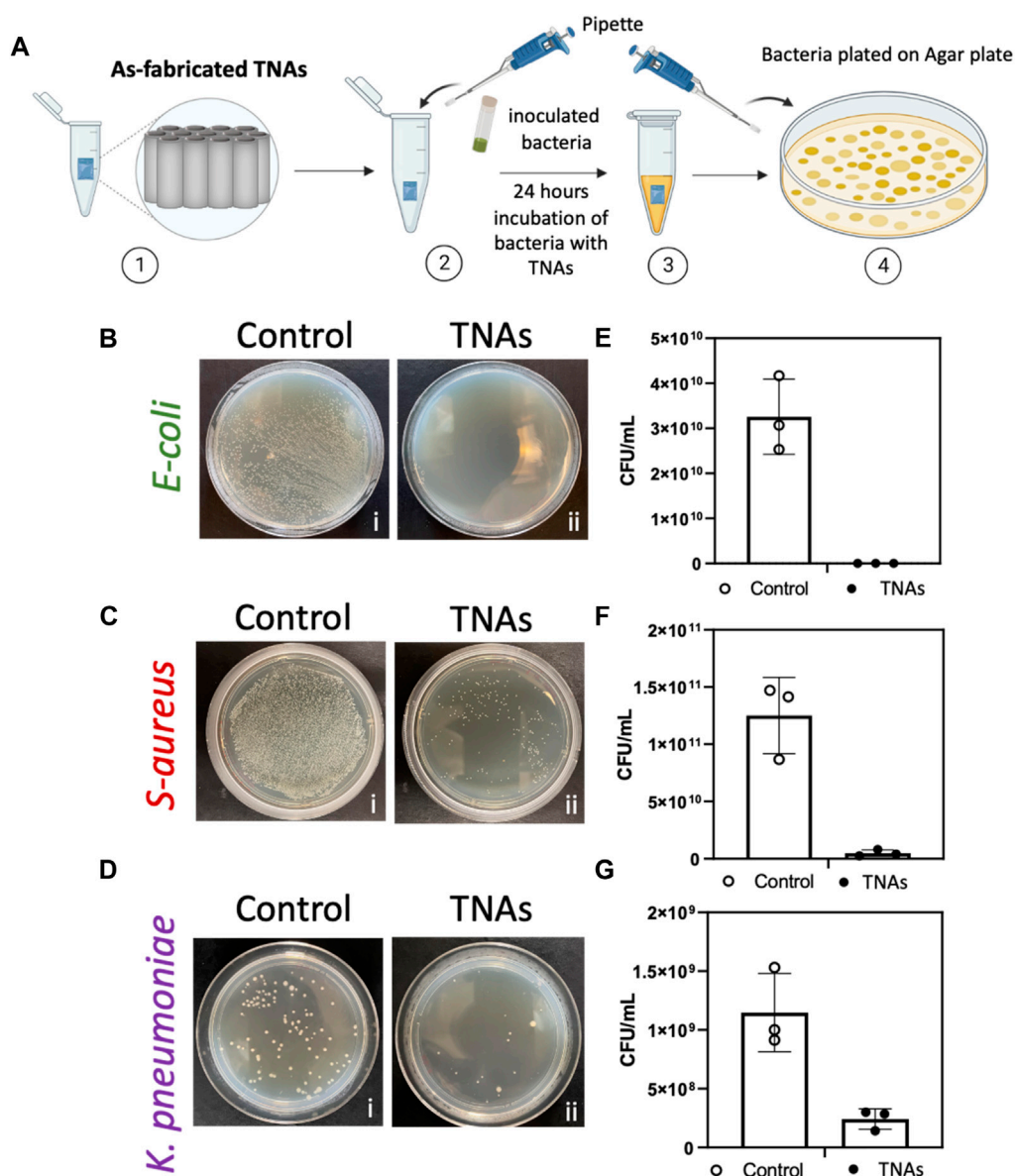
FIGURE 4
(A) Diagram of as-fabricated TNAs and bacteria incubation experiment; [1] as-fabricated TNAs placed in tube, [2] freshly inoculated bacteria added to the tube with as-fabricated TNAs, [3] bacteria and nanotubes incubated for 24 h, [4] bacteria plated in agar plate and incubated for 24 h before counting colony-forming units (CFU). Bacteria growth on an agar plate after 24-h incubation for **(B)** *E. coli*, b [i] control (bacteria only) and b [ii] incubated with TNAs, for **(C)** *Staphylococcus aureus*, c [i] control (bacteria only) and c [ii] incubated with TNAs, and for **(D)** *Klebsiella pneumoniae*, d [i] control (bacteria only) and d [ii] incubated with TNAs. Representation of the number of colony-forming units per milliliter (CFU. mL^{-1}) for control (bacteria only with no nanotubes) and after incubation with TNAs for **(E)** *E. coli*, **(F)** *Staphylococcus aureus*, and **(G)** *Klebsiella pneumoniae*, respectively. Data are expressed as mean $\pm$ standard deviation (n = 3).

4 Discussion

In light of the increasing prevalence of drug-resistant bacterial strains, conventional approaches such as systemic administration of antibiotics are proving detrimental over a long time and less effective in the treatment of bacterial infections (Fitzgerald, 2019). This has especially exacerbated the prevalence of infections related to implantable medical devices (Caplin and García, 2019). In this regard, a synergistic combination of antibacterial and bactericidal effects can be a promising strategy for preventing and treating bacterial infections in medical implants (Cyphert and von

Recum, 2017). It has been shown in several previous studies that TiO$_2$ nanotubes promote cell adhesion, differentiation and proliferation (such as osteoblast, stem and microglial cells) while inhibiting bacterial cell adhesion/growth (Crawford et al., 2007; Lan et al., 2013; Saha et al., 2021; Song et al., 2018; S. Wu et al., 2018). In this study, we fabricated TNAs through a two-step anodization process, with the aim of assessing the antibacterial efficacy of as-fabricated and antibiotic-loaded TNAs, against three different bacteria species from Gram-negative and Gram-positive bacterium types. The two-step anodization process (Figures 1A, B) created highly-ordered nanotubes of approximately 5 µm-length
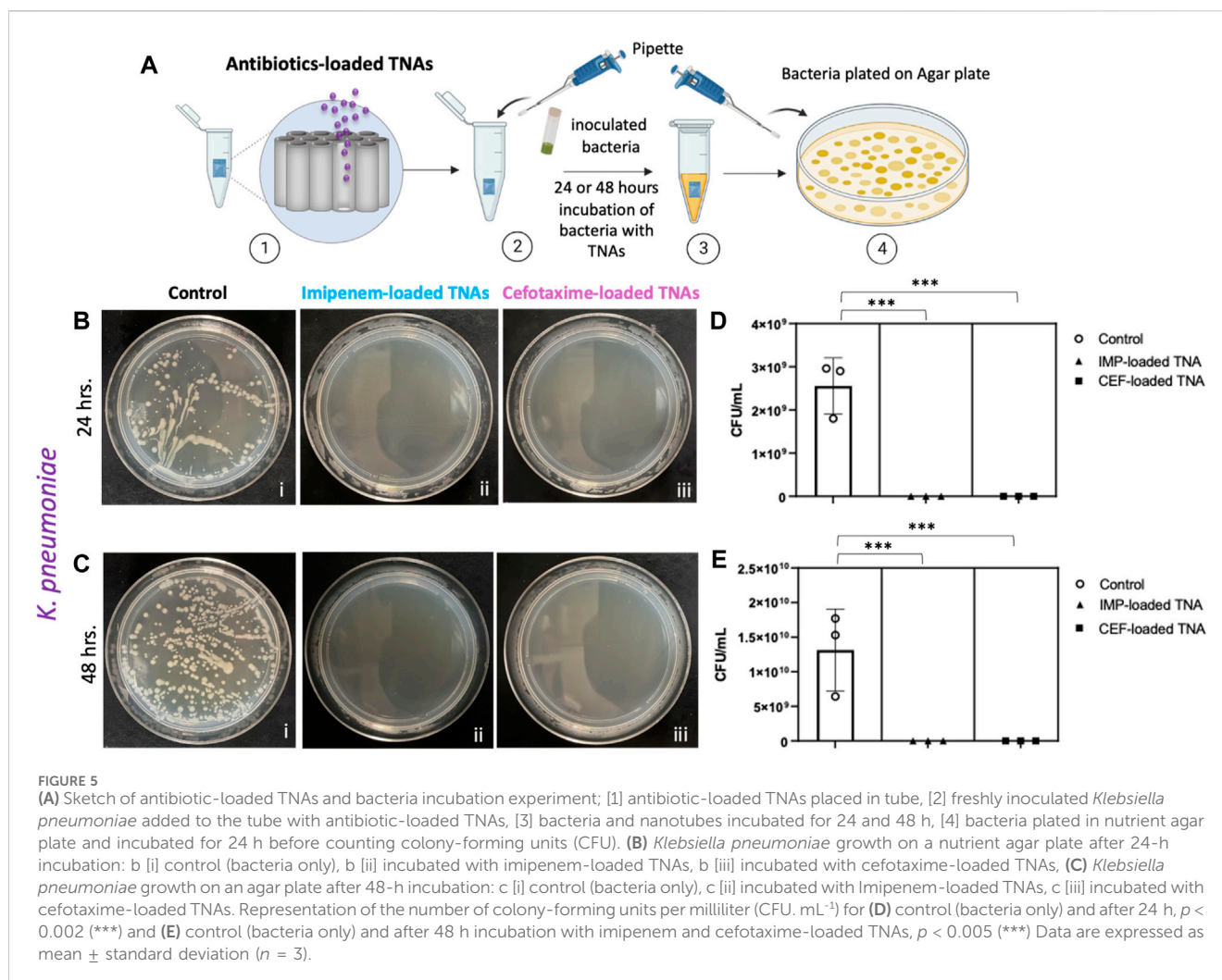
and 100 nm-diameter (Figures 1E–G) with a smoother surface as compared to one-step anodized nanotubes. The time-dependent application of voltage at the Ti anode and the electric charge flow impacts the anion transfer thus dictating the surface characteristics and dimensions of the TNAs. Two-step anodization process has been previously reported for the fabrication of debris-free highly-ordered TNAs (S. Li et al., 2009; Pishkar et al., 2018). Vertically-oriented nanotube arrays with different pore size and nanotube length can be fabricated by anodization as a coating on various substrates used for the development of implantable medical devices (Hamedani et al., 2014; Benčina et al., 2020; Amani Hamedani et al., 2023). Several mechanisms underlie the antibacterial activity of TNAs. Figures 2A, B illustrates that our TNAs surface contains ~15 At.% fluorine in the composition. Since this amount of fluorine is greater than that reported by (Tang et al., 2013) it is likely that the increased amount of fluorine on our TNAs enhances their antibacterial properties based on the studies by (Nurhaerani et al., 2006; Shinonaga and Arita, 2012) that demonstrated that fluorine boosts antibacterial activity. In an experiment on TiO_2 nanotubes, similar fluorine content was shown to increase bacterial adhesion, a finding confirmed by a few other studies on other materials (Puckett et al., 2010). Interestingly, Popat and colleagues have shown that the adhesion of bacteria can be decreased when the nanotubes are filled with an antibiotic (gentamicin) (Popat, Eltgroth, et al., 2007a). Therefore, different mechanism of action can be expected from the as-fabricated and antibiotic-loaded TNAs groups in terms of the effect of fluorine ion on the bacteria adhesion. Besides the composition, the nanotubular structure offers high surface area with nanoscale topography which could trigger destructive interactions with the extracellular matrix of bacteria while inhibiting their colonization, adhesion and proliferation (contact-killing) (Tang et al., 2013; Kunrath et al., 2019). Nanoscale roughness has been linked with increased bacterial adhesion and biofilm formation. Our AFM data revealed an average surface root-mean-square roughness (R_q) of 12.6 ± 1 nm for the two-step anodized TNAs (Figures 2C, D). A study reported increased bacterial adhesion and biofilm formation on nanostructured titania with R_q of up to 20 nm (Singh et al., 2011). As the roughness was further increased to 25 nm, bacterial adhesion and biofilm formation were significantly reduced. Based on the observations from other studies, our results suggest that fluorine content and roughness of the two-step anodized TNAs may have contributed to bacterial adhesion on the surface of as-fabricated TNAs. Nevertheless, a variety of other factors can influence bacterial behavior and adhesion to surfaces in response to their roughness, including the type of bacteria tested and the medium used which need to be accounted for precisely evaluating the effect of surface roughness on bacterial adhesion and the killing mechanism.

Further, functionalizing TNAs with biomolecules and metal nanoparticles can also enhance their performance through the release of metal ions that bond and disrupt the bacteria cell membranes on contact (Lan et al., 2013). Metal nanoparticles inactivate bacteria via production of reactive oxygen species (ROS), the same mechanism that causes cellular death in bactericidal antibiotics (Bedell et al., 2018). TNAs irradiated by UV light can generate ROS that have been reported to induce bacteria cell damage (Yamaguchi et al., 2020). TNA surface carries an electrostatic charge which affects the membrane

potential of the bacteria and impairs the survival function. Similar to metal ions, TNAs can release Ti^{3+} cations which interact with negatively charged species and disrupt bacteria protein and enzyme function, thus leading to bacterial death (ion-mediated killing) (Tavares et al., 2020).

As an additional benefit, the sustained localized delivery of antibiotics from TNAs can enhance their long-term antibacterial activity and promote a multifaceted bactericidal mechanism that can overcome resistance to antibiotics (Abe et al., 2015). A unique property of TNAs is the possibility for sequential filling of the nanotubes with multiple drugs for temporally controlled release of different drugs at various time points and for different durations. This will allow for utilizing a multidrug treatment approach for the treatment of invasive bacteria (Aw et al., 2012). In this study, cefotaxime and imipenem were loaded onto separate TNA samples to test the release of each drug independently. Our results revealed a controlled release of both antibiotics from TNAs (Figures 3A, B). In contrast to the studies by (Y. Li et al., 2019; Qin et al., 2014; Rathbone et al., 2011), we observed a slow release with no burst phase from the TNAs, likely due to their regulated nanotubular structure and the relative size of the drug molecule and the nanopores (Ferrati et al., 2013) thus minimizing the risk of toxicity from a burst release as well as enabling a prolonged release with the desired dosage.

Our bacterial assays were conducted using a slightly different process from previous studies–in which bacteria were directly cultured on TNAs (and their composites) surfaces–to simulate the conditions under which bacterial infections are introduced to the surgical site during the placement of an implantable medical device (Figure 4A). In this study the TNAs are placed in a tube and freshly inoculated bacteria is added to the same tube as a representation of an unsterile surgical procedure. This was in an effort to represent any bacteria which come in contact with the TNAs, no matter how brief. The TNAs and the bacteria are then incubated for at least 24 h and then the bacteria are plated on agar plates to visualize any effect of the TNAs on bacteria growth. All the bacteria assays were done in liquid media on a shaker incubator since *E. coli, S. aureus* and *K. pneumoniae* are all facultative anaerobic bacteria and can grow in both aerobic and anaerobic conditions (Trotter et al., 2011; Srinivasan et al., 2012; Missiakas and Schneewind, 2013). The shaking incubator mimics the internal environment of the body and fosters interaction between the TNAs and the bacteria. We observed that the as-fabricated TNAs alone suppressed *E. coli* growth (Figures 4B, E) and significantly reduced *S. aureus* growth (Figures 4C, F) after 24 h of incubation. However, the bactericidal activity of the as-fabricated TNAs was found to be much lower against *K. pneumoniae* (Figures 4D, G) post incubation. This disparity can likely be attributed to variations in bacterial cell wall structure, surface characteristics, and gene profile of *K. pneumoniae*, which possibly affect their sensitivity to the antibacterial effects of the as-fabricated TNAs (Amako et al., 1988). To the best of our knowledge, the antibacterial effects of TNAs on *K. pneumoniae* has not been previously investigated. Based on our results, the as-fabricated TNA exhibited the highest bactericidal activity against *E. coli* and *S. aureus*, the two bacteria that are often present in implant postoperative infections (Kunrath et al., 2019). This is in accordance with the study by Lan, et al. who reported similar antibacterial activity for silver-coated TiO_2

FIGURE 5
(A) Sketch of antibiotic-loaded TNAs and bacteria incubation experiment; [1] antibiotic-loaded TNAs placed in tube, [2] freshly inoculated *Klebsiella pneumoniae* added to the tube with antibiotic-loaded TNAs, [3] bacteria and nanotubes incubated for 24 and 48 h, [4] bacteria plated in nutrient agar plate and incubated for 24 h before counting colony-forming units (CFU). **(B)** *Klebsiella pneumoniae* growth on a nutrient agar plate after 24-h incubation: b [i] control (bacteria only), b [ii] incubated with imipenem-loaded TNAs, b [iii] incubated with cefotaxime-loaded TNAs, **(C)** *Klebsiella pneumoniae* growth on an agar plate after 48-h incubation: c [i] control (bacteria only), c [ii] incubated with Imipenem-loaded TNAs, c [iii] incubated with cefotaxime-loaded TNAs. Representation of the number of colony-forming units per milliliter (CFU. mL^{-1}) for **(D)** control (bacteria only) and after 24 h, $p <$ 0.002 (***) and **(E)** control (bacteria only) and after 48 h incubation with imipenem and cefotaxime-loaded TNAs, $p < 0.005$ (***) Data are expressed as mean $\pm$ standard deviation ($n = 3$).

nanotubes against *E. coli* and *S. aureus* (Lan et al., 2013). It is likely that the different surface morphology of the two-step anodized TNA played a role in hindering bacterial adhesion and thus inhibiting their growth. The antibacterial action of TNAs is multifaceted and depending on the type of bacteria, involves stretching of bacteria membranes and or surface charge repulsion dictated by variations in surface roughness. TNAs and most of bacteria, such as *E. coli* and *S. aureus*, both carry negative charges, which lead to repulsion and reduces bacterial adhesion (Y. Li et al., 2019). The stretch-forces generated by the TNA structure likely elevate pressure on the bacteria surface leading to membrane rupture. Surface roughness also affects surface wettability of the TNAs thus disrupting bacteria adhesion. TNAs antibacterial mechanisms are also closely tied to their dimensions. Changes in these dimensions can alter the forces that determine the antibacterial capabilities of TNAs. While there is no consensus on the relationship between TNAs diameter, roughness and antibacterial properties, our findings are consistent with recent studies (Tang et al., 2013; Simi and Rajendran, 2017) which demonstrate that larger diameters enhance antibacterial activity, as opposed to (Lewandowska et al., 2015; Radtke et al., 2017) who propose the opposite. Such discrepancies might be explained by differences in other

structural characteristics such as nanotube length, diameter, and wall thickness, which are outside the scope of this study.

Nevertheless, an integrated approach is desirable to maximize the synergistic effects of the TNAs' innate antibacterial activity and their ability for localized release of antibiotics to combat adaptation and development of drug-resistance from bacteria like *K. pneumoniae*. In its adaptation process, *K. pneumoniae* has the propensity to obtain iron more effectively from its surroundings. This likely boosts its capsule formation capabilities thus enhancing virulence and resistance (Amako et al., 1988). Therefore, we tested the antibacterial activity of cefotaxime- and imipenem-loaded TNAs against *K. pneumoniae*, which is previously shown to be susceptible to these two antibiotics (Cai et al., 2016; P. Chen et al., 2014). Both drugs have shown to operate by disrupting the synthesis of the bacteria cell walls (Bao et al., 2012). TNAs loaded with cefotaxime and imipenem were found to have 100% clearance of *K. pneumoniae* growth after 24 h (Figures 5B, D) and 48 h of incubation (Figures 5C, E), unlike previous studies like live Our results are likely due to the potentiated effects of antibiotics and the inherent antibacterial properties of TNAs. Chen et al. have reported the *in vivo* minimum inhibitory concentrations (MIC) of imipenem against *K. pneumoniae* (with introduced concentration of 10^6 CFU in the
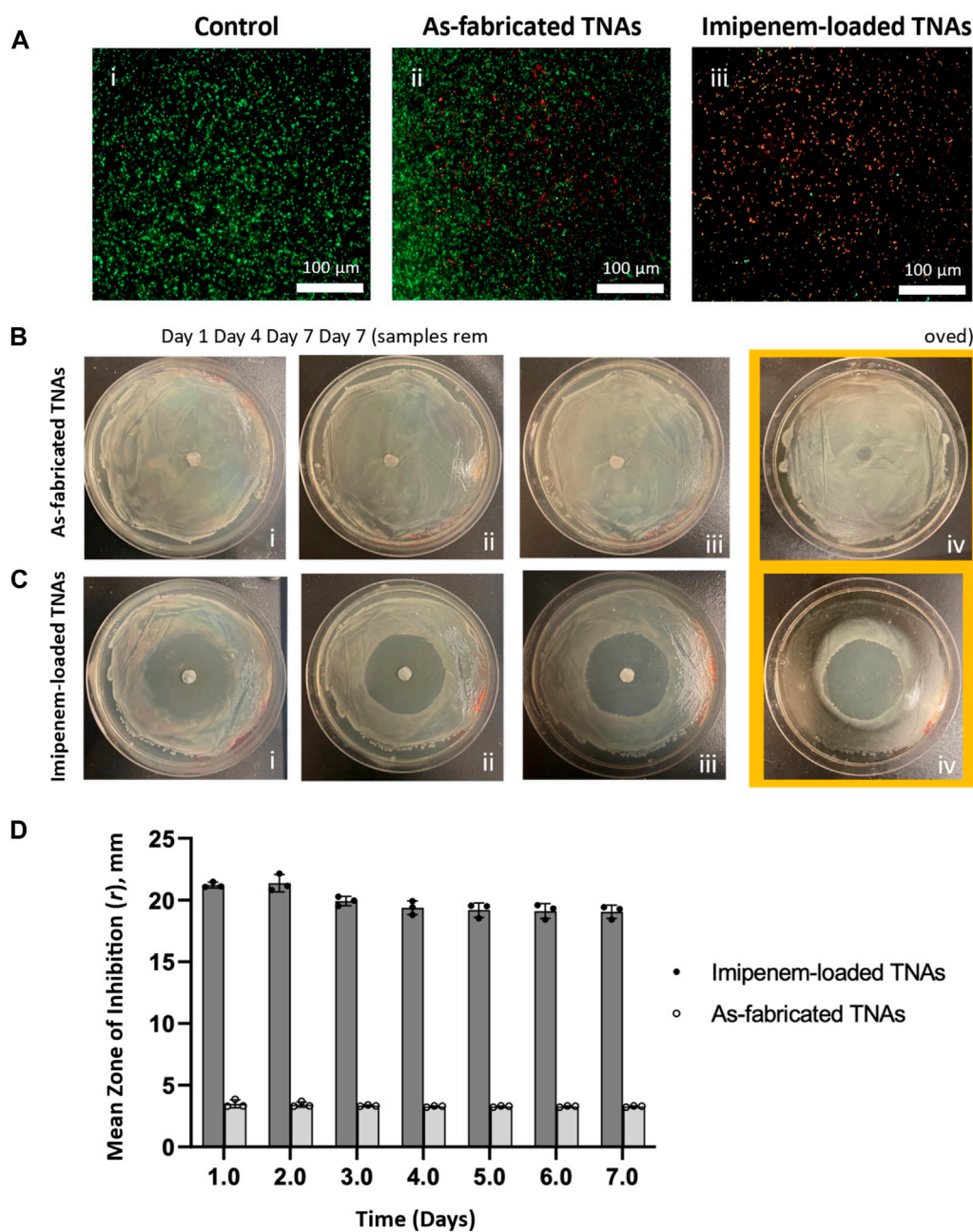
FIGURE 6
(A) Live/dead assay results: Fluorescence images of stained *Klebsiella pneumoniae* cells after 8-h: **[i]** control, **[ii]** incubation with as-fabricated and **[iii]** incubation with imipenem-loaded TNAs at 528 nm (green) for SYTO9 signal and 645 nm (red) for PI signal; bacteria exhibiting green fluorescence are considered live and the red or yellow fluorescence are considered dead bacteria (*n* = 3). Zone of inhibition for **(B)** as-fabricated and **(C)** imipenem-loaded TNAs against *Klebsiella pneumoniae* at: **[i]** day 1, **[ii]** day 4, **[iii]** day 7 of incubation and **[iv]** day 7 after removing the samples. **(D)** Plot showing the variations in mean radius of inhibition zone for as-fabricated and imipenem-loaded TNAs against *Klebsiella pneumoniae* over time. Data are expressed as mean ± standard deviation (*n* = 3).

biofilm-infected wounds) at 3.12 µg mL^{-1} reaching its maximum efficacy by completely destroying the biofilm at 25 µg. mL^{-1} (P. Chen et al., 2014). The concentrations of the imipenem released from the TNAs in the vials in this study were 10.27 µg mL^{-1} and 10.73 µg mL^{-1} after 24 h and 48 h of incubation with *K. pneumoniae*. Our *in vitro* bacterial assay results show that local release of imipenem from TNAs at the above concentrations can completely eradicate *K. pneumoniae* at a drastically higher initial concentration, *i.e.*,

1.23×10^{10} CFU. mL^{-1}. This is a significant result since the MICs obtained in this study is much lower than those reported by (Cai et al., 2016; Lee et al., 2021) in their investigations of the impact of cefotaxime against *K. pneumoniae*. Using the two-step anodization, highly-ordered TNAs with defined pores were formed, enabling the optimal dosage of cefotaxime to be used for local treatment of *K. pneumoniae*. The controlled release of antibiotic in combination with the TNAs' inherent antibacterial characteristics in this study

revealed to yield in a significant effect against a multidrug resistant bacterium in which lower doses of imipenem was found to be needed to treat the bacteria when used in combination with the antibacterial TNAs. A similar combined therapy approach was also explored by (Chhibber et al., 2017) and was found to be effective in lowering the antibiotic doses by using antibacterial silver nanoparticles with antibiotics against *K. pneumoniae*. The mechanism of action of the imipenem against *K. pneumoniae* biofilms is previously reported by a previous study as a clear change in characteristic morphology of bacteria, from rod to a sphere and ultimately fragmented (P. Chen et al., 2014). In their live/dead study, only a few individual live bacteria cells remained after the 5-h treatment with 25 µg. mL^{-1} imipenem. The results of our live/dead assay confirmed the synergistic antibacterial activity of antibiotic-loaded TNAs against *K. pneumoniae* within the first 8 h of incubation with *K. pneumoniae* (Figure 6A).

To qualitatively investigate how antibiotics synergize with the TNAs' inherent antibacterial properties, we performed a modified zone of inhibition assay, adapted from studies by (Halpern et al., 2014; Cyphert et al., 2018) over a 7-day period (Figures 6B–D). As seen in Figures 6Biv, Civ, a zone of inhibition was observed right beneath the TNA discs at the contact area to agar plate in both the as-fabricated and imipenem-loaded TNA groups after removing the samples from agar plates, which could be attributed to the inherent antibacterial activity of the TiO$_2$ nanotubes that resulted in inhibiting bacterial growth in the zone of contact with TNAs (contact-killing) (Kunrath et al., 2019; Saha et al., 2021). However, a significantly larger zone of inhibition (a circular area surrounding the discs) was found in the imipenem-loaded TNA samples which confirms that the growth of *K. pneumoniae* was considerably restricted possibly due to the slow-release of imipenem from the TNAs. The synergistic effect was observed to last for at least 7 days before the medium dried out. This suggests that the antibacterial activity of implant devices coated with antibiotic-loaded TNAs can be possibly sustained over a longer period of time *in vivo* (where the physiological environment surrounding the implant maintain the hydrated condition for antibiotic release) by providing a well-defined zone of inhibition around the implant. Furthermore, in our study, with ~10 µg. mL^{-1} of antibiotic released from the TNAs, the zone size difference over the control was nearly 18 mm. This result far exceeds the zone difference observed in the research conducted by (S. Roy et al., 2010). In that study, zone of inhibition assay was employed to assess the impact of titanium dioxide nanoparticles impregnated with several antibiotic against *S. aureus*, wherein different dosages of antibiotics loaded into TiO$_2$ nano-discs resulted in the zone size differences varying from 2 to 10 mm compared to non-loaded TiO$_2$ nano-discs.

Our results highlight the potential of TNAs as an antibacterial means for the local administration of antibiotics to treat bacterial infections related to implantable medical devices. Incorporating antibiotics into TNAs offers a promising strategy for overcoming bacterial resistance and improving the efficacy of antimicrobial treatments. Additionally, this strategy expands the antibiotic options to include those previously known to be resisted by bacteria. Furthermore, the controlled release of antibiotics from TNAs could minimize systemic exposure, reduce the risk of side effects, and promote targeted therapy. Generally, the development of TiO$_2$-based technologies has huge implications for preventing and managing bacterial infections in implanted medical devices, as well as reduce the risk of development of antibacterial resistance (Qiu et al., 2015; Ge et al., 2019). However, further investigation is warranted in order to 1) understand the underlying mechanisms that contribute to the TNAs antibacterial activity, 2) optimize the TNAs for enhanced antibacterial efficacy and against a broader spectrum of infectious bacteria including *Enterococcus faecalis, Pseudomonas aeruginosa, and Propionibacterium acnes* which are also commonly associated with implantable medical devices, 3) study the effect of TNAs and antibiotics in polymicrobial infection models, which better represent the clinical scenario, and 4) evaluate the long term efficacy of the TNAs in both preclinical and clinical settings.

5 Conclusion

This study investigated the antibacterial activity of TNAs fabricated via two-step electrochemical anodization process, and then either loaded or not loaded with antibiotics, against *E. coli* and *S. aureus, and K. pneumoniae* bacteria. The as-fabricated TNAs were found to inhibit the growth of *E. coli* (100% clearance) and significantly reduced *S. aureus* growth (97% clearance) after 24 h of incubation. Moreover, TNAs loaded with imipenem and cefotaxime demonstrated a sustained and slow-release profile *in vitro* and exhibited remarkable antibacterial activity against *K. pneumoniae* by inhibiting their growth (100% clearance) during 24 and 48 h of incubation which was maintained for 7 days. With ~10 µg. mL^{-1} of antibiotic released from the TNAs, the zone size difference over the control was nearly 18 mm. These findings support the potential of TNAs for both early-stage prevention and long-term inhibition of bacterial infections at the implant site by combating the most clinically-relevant Gram-positive and Gram-negative strains of bacteria via local delivery of broad-spectrum antibiotics. By combining their inherent antibacterial properties with the capability for controlled and sustained release of antibiotics, TNAs are more effective than conventional methods for the treatment of implant-related bacterial infections. Specifically, the biocompatibility and versatility of TNAs in loading and releasing multiple drugs open up the possibility of using them as a multifunctional coating on implantable devices for sustained and localized release of a wide range of antibiotics at lower dosages from the implants, which would lead to a comprehensive solution to combat multidrug resistance without causing toxicity in non-target organs.

Data availability statement

The data supporting the conclusion of this article will be made available on request from the corresponding author, HA.

Author contributions

EO: Writing–original draft, Investigation, Data curation, Conceptualization. HW: Methodology, Writing–original draft. JC: Supervision, Resources, Funding acquisition, Writing–review and editing. HvR: Conceptualization, Writing–review and editing, Supervision, Resources, Funding acquisition. HA:

Writing–original draft, Visualization, Validation, Software, Project administration, Methodology, Investigation, Formal Analysis, Data curation, Writing–review and editing, Supervision, Resources, Funding acquisition, Conceptualization.

Conflict of interest

The authors declare that the research was conducted in the absence of any commercial or financial relationships that could be construed as a potential conflict of interest.

The author(s) declared that they were an editorial board member of Frontiers, at the time of submission. This had no impact on the peer review process and the final decision.

Publisher's note

All claims expressed in this article are solely those of the authors and do not necessarily represent those of their affiliated organizations, or those of the publisher, the editors and the reviewers. Any product that may be evaluated in this article, or claim that may be made by its manufacturer, is not guaranteed or endorsed by the publisher.

Author disclaimer

The contents do not represent the views of the U.S. Department of Veterans Affairs, the National Institutes of Health, or the United States Government.

References

Abel, S., Moom Sinn, Aw, Bariana, M., Kumeria, T., Wang, Ye, and Losic, D. (2015). Titania nanotube arrays for local drug delivery: recent advances and perspectives. *Expert Opin. Drug Deliv.* 12 (Issue 1), 103–127. doi:10.1517/17425247.2014.945418

Amako, K., Meno, Y., and Takade, A. (1988). Fine structures of the capsules of *Klebsiella pneumoniae* and *Escherichia coli* K1. *J. Bacteriol.* 170 (10), 4960–4962. doi:10.1128/jb.170.10.4960-4962.1988

Amani Hamedani, H., Stegall, T., Yang, Y., Wang, H., Menon, A., Bhalotia, A., et al. (2023). Flexible multifunctional titania nanotube array platform for biological interfacing. *MRS Bull.* doi:10.1557/s43577-023-00628-y

Aw, M. S., Addai-Mensah, J., and Losic, D. (2012). A multi-drug delivery system with sequential release using titania nanotube arrays. *Chem. Commun.* 48 (27), 3348–3350. doi:10.1039/c2cc17690d

Bao, L., Peng, R., Ren, X., Ma, R., Li, J., and Wang, Y. (2012). Analysis of some common pathogens and their drug resistance to antibiotics. *Pak. J. Med. Sci.* 29 (1), 135–139. doi:10.12669/pjms.291.2744

Baptista, P. V., McCusker, M. P., Carvalho, A., Ferreira, D. A., Mohan, N. M., Martins, M., et al. (2018). Nano-strategies to fight multidrug resistant bacteria—"A battle of the titans.". *Front. Microbiol.* 9, 1441. doi:10.3389/fmicb.2018.01441

Bassetti, M., and Righi, E. (2020). Overcoming antibiotic resistance: new perspectives. 457–480. doi:10.1007/978-3-030-32857-3_19

Bedell, H. W., Song, S., Li, X., Molinich, E., Lin, S., Stiller, A., et al. (2018). Understanding the effects of both CD14-mediated innate immunity and device/tissue mechanical mismatch in the neuroinflammatory response to intracortical microelectrodes. *Front. Neurosci.* 12, 772. doi:10.3389/fnins.2018.00772

Benčina, M., Iglič, A., Mozetič, M., and Junkar, I. (2020). Crystallized TiO2 nanosurfaces in biomedical applications. *Nanomaterials* 10 (Issue 6), 1121. doi:10.3390/nano10061121

Bowden, L. C., Evans, J. G. W., Miller, K. M., Bowden, A. E., Jensen, B. D., Hope, S., et al. (2023). Carbon-infiltrated carbon nanotubes inhibit the development of *Staphylococcus aureus* biofilms. *Sci. Rep.* 13 (1), 19398. doi:10.1038/s41598-023-46748-y

Cai, W., Fu, Y., Zhang, W., Chen, X., Zhao, J., Song, W., et al. (2016). Synergistic effects of baicalein with cefotaxime against *Klebsiella pneumoniae* through inhibiting CTX-M-1 gene expression. *BMC Microbiol.* 16 (1), 181. doi:10.1186/s12866-016-0797-1

Caplin, J. D., and García, A. J. (2019). Implantable antimicrobial biomaterials for local drug delivery in bone infection models. *Acta Biomater.* 93, 2–11. doi:10.1016/j.actbio.2019.01.015

Chen, L., Song, X., Xing, F., Wang, Y., Wang, Y., He, Z., et al. (2020). A review on antimicrobial coatings for biomaterial implants and medical devices. *J. Biomed. Nanotechnol.* 16 (6), 789–809. doi:10.1166/jbn.2020.2942

Chen, P., Seth, A. K., Abercrombie, J. J., Mustoe, T. A., and Leung, K. P. (2014). Activity of imipenem against *Klebsiella pneumoniae* biofilms *in vitro* and *in vivo*. *Antimicrob. Agents Chemother.* 58 (2), 1208–1213. doi:10.1128/AAC.01353-13

Chhibber, S., Gondil, V. S., Sharma, S., Kumar, M., Wangoo, N., and Sharma, R. K. (2017). A novel approach for combating *Klebsiella pneumoniae* biofilm using histidine functionalized silver nanoparticles. *Front. Microbiol.* 8 (JUN), 1104. doi:10.3389/fmicb.2017.01104

Costa, F. S. L., Bezerra, C. C. R., Neto, R. M., Morais, C. L. M., and Lima, K. M. G. (2020). Identification of resistance in *Escherichia coli* and *Klebsiella pneumoniae* using excitation-emission matrix fluorescence spectroscopy and multivariate analysis. *Sci. Rep.* 10 (1), 12994. doi:10.1038/s41598-020-70033-x

Crawford, G. A., Chawla, N., Das, K., Bose, S., and Bandyopadhyay, A. (2007). Microstructure and deformation behavior of biocompatible TiO2 nanotubes on titanium substrate. *Acta Biomater.* 3 (3), 359–367. doi:10.1016/j.actbio.2006.08.004

Cyphert, E. L., Learn, G. D., Hurley, S. K., Lu, C., and von Recum, H. A. (2018). An additive to PMMA bone cement enables postimplantation drug refilling, broadens range of compatible antibiotics, and prolongs antimicrobial therapy. *Adv. Healthc. Mater.* 7 (21), e1800812. doi:10.1002/adhm.201800812

Cyphert, E. L., and von Recum, H. A. (2017). Emerging technologies for long-term antimicrobial device coatings: advantages and limitations. *Exp. Biol. Med.* 242 (8), 788–798. doi:10.1177/1535370216688572

Darouiche, R. O. (2007). Antimicrobial coating of devices for prevention of infection: principles and protection. *Int. J. Artif. Organs* 30 (9), 820–827. doi:10.1177/039139880703000912

Dizaj, S. M., Lotfipour, F., Barzegar-Jalali, M., Zarrintan, M. H., and Adibkia, K. (2014). Antimicrobial activity of the metals and metal oxide nanoparticles. *Mater. Sci. Eng. C* 44, 278–284. doi:10.1016/j.msec.2014.08.031

Doron, S., and Gorbach, S. L. (2008). "Bacterial infections: overview," in *International encyclopedia of public health* (Elsevier), 273–282. doi:10.1016/B978-012373960-5. 00596-7

Draghi, L., Preda, V., Moscatelli, M., Santin, M., and Chiesa, R. (2020). Gentamicin-loaded TiO2 nanotubes as improved antimicrobial surfaces for orthopedic implants. *Front. Mater.* 7. doi:10.3389/fmats.2020.00233

Fair, R. J., and Tor, Y. (2014). Antibiotics and bacterial resistance in the 21st century. *Perspect. Med. Chem.*, 6, S14459. doi:10.4137/PMC.S14459

Ferrati, S., Fine, D., You, J., Rosa, E.De, Hudson, L., Zabre, E., et al. (2013). Leveraging nanochannels for universal, zero-order drug delivery *in vivo*. *J. Control. Release* 172 (3), 1011–1019. doi:10.1016/j.jconrel.2013.09.028

Fitzgerald, D. M. (2019). Bacterial Evolution: the road to resistance. *ELife* 8, e52092. doi:10.7554/eLife.52092

Ge, X., Ren, C., Ding, Y., Chen, G., Lu, X., Wang, K., et al. (2019). Micro/nano-structured TiO2 surface with dual-functional antibacterial effects for biomedical applications. *Bioact. Mater.* 4, 346–357. doi:10.1016/j.bioactmat.2019.10.006

Gulati, K., Kogawa, M., Maher, S., Atkins, G., Findlay, D., and Losic, D. (2015).Titania nanotubes for local drug delivery from implant surfaces. *Springer Ser. Mater. Sci.*, 220, 307–355. doi:10.1007/978-3-319-20346-1_10

Halpern, J. M., Gormley, C. A., Keech, M. A., and von Recum, H. A. (2014). Thermomechanical properties, antibiotic release, and bioactivity of a sterilized cyclodextrin drug delivery system. *J. Mater. Chem. B* 2 (18), 2764–2772. doi:10. 1039/C4TB00083H

Hamedani, H. A., Khaleel, J. A., Dahmen, K. H., and Garmestani, H. (2014). Surface controlled growth of thin-film strontium titanate nanotube arrays on silicon. *Cryst. Growth Des.* 14 (10), 4911–4919. doi:10.1021/cg500374m

Hetta, H. F., Ramadan, Y. N., Al-Harbi, A. I., Ahmed, E., Battah, B., Abd Ellah, N. H., et al. (2023). Nanotechnology as a promising approach to combat multidrug resistant bacteria: a comprehensive review and future perspectives. *Biomedicines* 11 (2), 413. doi:10.3390/biomedicines11020413

Jafari, S., Mahyad, B., Hashemzadeh, H., Janfaza, S., Gholikhani, T., and Tayebi, L. (2020). <p>Biomedical Applications of TiO₂ Nanostructures: recent Advances</p>. *Int. J. Nanomedicine* 15, 3447–3470. doi:10.2147/IJN.S249441

JankauskaitŁ, V., VitkauskienŁ, A., Lazauskas, A., Baltrusaitis, J., ProsyŁevas, I., and AndruleviŁius, M. (2016). Bactericidal effect of graphene oxide/Cu/Ag nanoderivatives against *Escherichia coli*, *Pseudomonas aeruginosa*, *Klebsiella pneumoniae*, *Staphylococcus aureus* and Methicillin-resistant *Staphylococcus aureus*. *Int. J. Pharm.* 511 (1), 90–97. doi:10.1016/j.ijpharm.2016.06.121

Jepsen, K., and Jepsen, S. (2016). Antibiotics/antimicrobials: systemic and local administration in the therapy of mild to moderately advanced periodontitis. *Periodontol. 2000* 71 (1), 82–112. doi:10.1111/prd.12121

Khatoon, Z., McTiernan, C. D., Suuronen, E. J., Mah, T.-F., and Alarcon, E. I. (2018). Bacterial biofilm formation on implantable devices and approaches to its treatment and prevention. *Heliyon* 4 (12), e01067. doi:10.1016/j.heliyon.2018.e01067

Kumaravel, V., Nair, K. M., Mathew, S., Bartlett, J., Kennedy, J. E., Manning, H. G., et al. (2021). Antimicrobial TiO2 nanocomposite coatings for surfaces, dental and orthopaedic implants. *Chem. Eng. J.* 416, 129071. doi:10.1016/j.cej.2021.129071

Kunrath, M. F., Leal, B. F., Hubler, R., de Oliveira, S. D., and Teixeira, E. R. (2019). Antibacterial potential associated with drug-delivery built TiO2 nanotubes in biomedical implants. *Amb. Express* 9 (1), 51. doi:10.1186/s13568-019-0777-6

Lan, M.-Y., Liu, C.-P., Huang, H.-H., and Lee, S.-W. (2013). Both enhanced biocompatibility and antibacterial activity in Ag-decorated TiO2 nanotubes. *PLoS ONE* 8 (10), e75364. doi:10.1371/journal.pone.0075364

Lee, D., Oh, J. Y., Sum, S., and Park, H.-M. (2021). Prevalence and antimicrobial resistance of *Klebsiella* species isolated from clinically ill companion animals. *J. Veterinary Sci.* 22 (2), e17. doi:10.4142/jvs.2021.22.e17

Lewandowska, Ż., Piszczek, P., Radtke, A., Jędrzejewski, T., Kozak, W., and Sadowska, B. (2015). The evaluation of the impact of titania nanotube covers morphology and crystal phase on their biological properties. *J. Mater. Sci. Mater. Med.* 26 (4), 163–212. doi:10.1007/s10856-015-5495-2

Li, S., Zhang, G., Guo, D., Yu, L., and Zhang, W. (2009). Anodization fabrication of highly ordered TiO$_2$ nanotubes. *J. Phys. Chem. C* 113 (29), 12759–12765. doi:10.1021/jp903037f

Li, Y., Yang, Y., Li, R., Tang, X., Guo, D., Qing, Y., et al. (2019). Enhanced antibacterial properties of orthopedic implants by titanium nanotube surface modification: a review of current techniques. *Int. J. Nanomedicine* 14, 7217–7236. doi:10.2147/IJN.S216175

Makabenta, J. M. V., Nabawy, A., Li, C. H., Schmidt-Malan, S., Patel, R., and Rotello, V. M. (2021). Nanomaterial-based therapeutics for antibiotic-resistant bacterial infections. *Nat. Rev. Microbiol.* 19 (1), 23–36. doi:10.1038/S41579-020-0420-1

Martinez, J. L., and Baquero, F. (2000). Mutation frequencies and antibiotic resistance. *Antimicrob. Agents Chemother.* 44 (Issue 7), 1771–1777. doi:10.1128/aac.44.7.1771-1777.2000

Medina, E., and Pieper, D. H. (2016). Tackling threats and future problems of multidrug-resistant bacteria. *Curr. Top. Microbiol. Immunol.* 398, 3–33. doi:10.1007/82_2016_492

Mei, S., Wang, H., Wang, W., Tong, L., Pan, H., Ruan, C., et al. (2014). Antibacterial effects and biocompatibility of titanium surfaces with graded silver incorporation in titania nanotubes. *Biomaterials* 35 (14), 4255–4265. doi:10.1016/j.biomaterials.2014. 02.005

Missiakas, D. M., and Schneewind, O. (2013). Growth and laboratory maintenance of *Staphylococcus aureus*. *Curr. Protoc. Microbiol.* 28 (1), Unit 9C.1. doi:10.1002/9780471729259.mc09c01s28

Nurhaerani, Arita, K., Shinonaga, Y., and Nishino, M. (2006). Plasma-based fluorine ion implantation into dental materials for inhibition of bacterial adhesion. *Dent. Mater. J.* 25 (4), 684–692. doi:10.4012/DMJ.25.684

Pishkar, N., Ghoranneviss, M., Ghorannevis, Z., and Akbari, H. (2018). Study of the highly ordered TiO2 nanotubes physical properties prepared with two-step anodization. *Results Phys.* 9, 1246–1249. doi:10.1016/j.rinp.2018.02.009

Popat, K. C., Eltgroth, M., LaTempa, T. J., Grimes, C. A., and Desai, T. A. (2007a). Decreased *Staphylococcus epidermis* adhesion and increased osteoblast functionality on antibiotic-loaded titania nanotubes. *Biomaterials* 28 (32), 4880–4888. doi:10.1016/j. biomaterials.2007.07.037

Popat, K. C., Eltgroth, M., LaTempa, T. J., Grimes, C. A., and Desai, T. A. (2007b). Titania nanotubes: a novel platform for drug-eluting coatings for medical implants? *Small* 3 (11), 1878–1881. doi:10.1002/smll.200700412

Popat, K. C., Leoni, L., Grimes, C. A., and Desai, T. A. (2007). Influence of engineered titania nanotubular surfaces on bone cells. *Biomaterials* 28 (21), 3188–3197. doi:10. 1016/j.biomaterials.2007.03.020

Pray, L. (2008). *Antibiotic resistance, mutation rates and MRSA*.

Puckett, S. D., Taylor, E., Raimondo, T., and Webster, T. J. (2010). The relationship between the nanostructure of titanium surfaces and bacterial attachment. *Biomaterials* 31 (4), 706–713. doi:10.1016/j.biomaterials.2009.09.081

Qin, H., Cao, H., Zhao, Y., Zhu, C., Cheng, T., Wang, Q., et al. (2014). *In vitro* and *in vivo* anti-biofilm effects of silver nanoparticles immobilized on titanium. *Biomaterials* 35 (33), 9114–9125. doi:10.1016/J.BIOMATERIALS.2014.07.040

Qiu, Z., Shen, Z., Qian, D., Jin, M., Yang, D., Wang, J., et al. (2015). Effects of nano-TiO$_2$ on antibiotic resistance transfer mediated by RP4 plasmid. *Nanotoxicology* 9 (7), 895–904. doi:10.3109/17435390.2014.991429

Radtke, A., Topolski, A., Jędrzejewski, T., Kozak, W., Sadowska, B., Więckowska-Szakiel, M., et al. (2017). The bioactivity and photocatalytic properties of titania nanotube coatings produced with the use of the low-potential anodization of Ti6Al4V alloy surface. *Nanomaterials* 7 (8), 197. doi:10.3390/NANO7080197

Rathbone, C. R., Cross, J. D., Brown, K. V., Murray, C. K., and Wenke, J. C. (2011). Effect of various concentrations of antibiotics on osteogenic cell viability and activity. *J. Orthop. Res.* 29 (7), 1070–1074. doi:10.1002/JOR.21343

Roy, P., Berger, S., and Schmuki, P. (2011). TiO2 nanotubes: synthesis and applications. *Angew. Chem. Int. Ed.* 50 (13), 2904–2939. doi:10.1002/anie. 201001374

Roy, S. A., Parveen, A., Koppalkar, A. R., and Prasad, A. (2010). Effect of nano - titanium dioxide with different antibiotics against methicillin-resistant Staphylococcus aureus. *J. Biomaterials Nanobiotechnology* 01 (01), 37–41. doi:10.4236/JBNB.2010. 11005

Saha, S., Pramanik, K., and Biswas, A. (2021). Antibacterial activity and biocompatibility of curcumin/TiO$_2$ nanotube array system on Ti6Al4V bone implants. *Mater. Technol.* 36 (4), 221–232. doi:10.1080/10667857.2020.1742984

Sekhon, T. K., and Sekhon, B. S. (2021). Local drug delivery: a brief review. *Mar. Dent. Sci.* 2 (4).

Shinonaga, Y., and Arita, K. (2012). Antibacterial effect of acrylic dental devices after surface modification by fluorine and silver dual-ion implantation. *Acta Biomater.* 8 (3), 1388–1393. doi:10.1016/J.ACTBIO.2011.09.017

Simi, V. S., and Rajendran, N. (2017). Influence of tunable diameter on the electrochemical behavior and antibacterial activity of titania nanotube arrays for biomedical applications. *Mater. Charact.* 129, 67–79. doi:10.1016/J.MATCHAR.2017. 04.019

Singh, A. V., Vyas, V., Patil, R., Sharma, V., Scopelliti, P. E., Bongiorno, G., et al. (2011). Quantitative characterization of the influence of the nanoscale morphology of nanostructured surfaces on bacterial adhesion and biofilm formation. *PLoS ONE* 6 (9), e25029. doi:10.1371/journal.pone.0025029

Song, R., Zhang, Y., Huang, Q., Yang, Y., Lin, L., Liang, J., et al. (2018). Facile construction of structural gradient of TiO$_2$ nanotube arrays on medical titanium for high throughput evaluation of biocompatibility and antibacterial property. *ACS Appl. Bio Mater.* 1 (4), 1056–1065. doi:10.1021/acsabm.8b00288

Srinivasan, V. B., Vaidyanathan, V., Mondal, A., and Rajamohan, G. (2012). Role of the two component signal transduction system CpxAR in conferring cefepime and chloramphenicol resistance in *Klebsiella pneumoniae* NTUH-K2044. *PLoS ONE* 7 (4), e33777. doi:10.1371/journal.pone.0033777

Tang, T., Peng, N, Zheng, K., Wang He, Jin, S., Wang, X., et al. (2013). Dual effects and mechanism of TiO2 nanotube arrays in reducing bacterial colonization and enhancing C3H10T1/2 cell adhesion. *Int. J. Nanomedicine* 3093, 3093. doi:10.2147/IJN.S48084

Tavares, T. D., Antunes, J. C., Padrão, J., Ribeiro, A. I., Zille, A., Amorim, M. T. P., et al. (2020). Activity of specialized biomolecules against gram-positive and gram-negative bacteria. *Antibiotics* 9 (6), 314. doi:10.3390/antibiotics9060314

ter Boo, G.-J. A., Grijpma, D. W., Moriarty, T. F., Richards, R. G., and Eglin, D. (2015). Antimicrobial delivery systems for local infection prophylaxis in orthopedic- and trauma surgery. *Biomaterials* 52, 113–125. doi:10.1016/j.biomaterials.2015.02.020

Trotter, E. W., Rolfe, M. D., Hounslow, A. M., Craven, C. J., Williamson, M. P., Sanguinetti, G., et al. (2011). Reprogramming of *Escherichia coli* K-12 metabolism during the initial phase of transition from an anaerobic to a micro-aerobic environment. *PLoS ONE* 6 (9), e25501. doi:10.1371/journal.pone.0025501

VanEpps, J. S., and Younger, J. G. (2016). Implantable device-related infection. *Shock* 46 (6), 597–608. doi:10.1097/SHK.0000000000000692

von Eiff, C., Jansen, B., Kohnen, W., and Becker, K. (2005a). Infections associated with medical devices. *Drugs* 65 (2), 179–214. doi:10.2165/00003495-200565020-00003

Von Eiff, C., Kohnen, W., Becker, K., and Jansen, B. (2005b). Modern strategies in the prevention of implant-associated infections. *Int. J. Artif. Organs* 28 (11), 1146–1156. doi:10.1177/039139880502801112

Wang, Q., Huang, J. Y., Li, H. Q., Chen, Z., Zhao, A. Z. J., Wang, Y., et al. (2016). "TiO2 nanotube platforms for smart drug delivery: a review," in *International journal of nanomedicine* (Macclesfield, United Kingdom: Dove Medical Press Ltd), 11, 4819–4834. doi:10.2147/IJN.S108847

Wu, S., Zhang, B., Liu, Y., Suo, X., and Li, H. (2018). Influence of surface topography on bacterial adhesion: a review (Review). *Biointerphases* 13 (6), 060801. doi:10.1116/1.5054057

Wu, Z.-L., Zhao, J., and Xu, R. (2020). Recent advances in oral nano-antibiotics for bacterial infection therapy. *Int. J. Nanomedicine* 15, 9587–9610. doi:10.2147/IJN.S279652

Yamaguchi, M., Abe, H., Ma, T., Tadaki, D., Hirano-Iwata, A., Kanetaka, H., et al. (2020). Bactericidal activity of TiO$_2$ nanotube thin films on Si by photocatalytic generation of active oxygen species. *Langmuir* 36 (42), 12668–12677. doi:10.1021/acs.langmuir.0c02225

Zhao, L., Wang, H., Huo, K., Cui, L., Zhang, W., Ni, H., et al. (2011). Antibacterial nano-structured titania coating incorporated with silver nanoparticles. *Biomaterials* 32 (24), 5706–5716. doi:10.1016/j.biomaterials.2011.04.040

Zheng, S., Bawazir, M., Dhall, A., Kim, H.-E., He, L., Heo, J., et al. (2021). Implication of surface properties, bacterial motility, and hydrodynamic conditions on bacterial surface sensing and their initial adhesion. *Front. Bioeng. Biotechnol.* 9, 643722. doi:10.3389/fbioe.2021.643722